

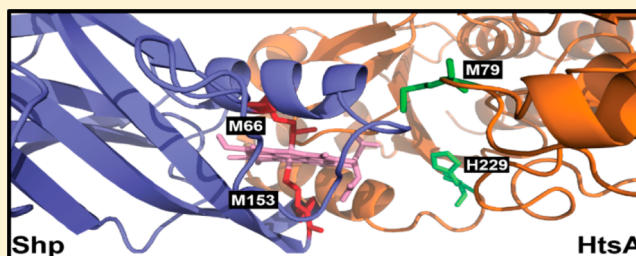
Axial Ligand Replacement Mechanism in Heme Transfer from Streptococcal Heme-Binding Protein Shp to HtsA of the HtsABC Transporter

Yanchao Ran,^{†,§} G. Reza Malmirchegini,[‡] Robert T. Clubb,[‡] and Benfang Lei^{*,†}

[†]Department of Immunology and Infectious Diseases, Montana State University, Bozeman, Montana 59718, United States

[‡]Department of Chemistry and Biochemistry, University of California, Los Angeles, California 90095, United States

ABSTRACT: The heme-binding protein Shp of Group A *Streptococcus* rapidly transfers its heme to HtsA, the lipoprotein component of the HtsABC transporter, in a concerted two-step process with one kinetic phase. Heme axial residue-to-alanine replacement mutant proteins of Shp and HtsA (Shp^{M66A}, Shp^{M153A}, HtsA^{M79A}, and HtsA^{H229A}) were used to probe the axial displacement mechanism of this heme transfer reaction. Ferric Shp^{M66A} at high pH and Shp^{M153A} have a pentacoordinate heme iron complex with a methionine axial ligand. ApoHtsA^{M79A} efficiently acquires heme from ferric Shp but alters the reaction mechanism to two kinetic phases from a single phase in the wild-type protein reactions. In contrast, apoHtsA^{H229A} cannot assimilate heme from ferric Shp. The conversion of pentacoordinate holoShp^{M66A} into pentacoordinate holoHtsA^{H229A} involves an intermediate, whereas holoHtsA^{H229A} is directly formed from pentacoordinate holoShp^{M153A}. Conversely, apoHtsA^{M79A} reacts with holoShp^{M66A} and holoShp^{M153A} in mechanisms with one and two kinetic phases, respectively. These results imply that the Met79 and His229 residues of HtsA displace the Met66 and Met153 residues of Shp, respectively. Structural docking analysis supports this mechanism of the specific axial residue displacement. Furthermore, the rates of the cleavage of the axial bond in Shp in the presence of a replacing HtsA axial residue are greater than that in the absence of a replacing HtsA axial residue. These findings reveal a novel heme transfer mechanism of the specific displacement of the Shp axial residues with the HtsA axial residues and the involvement of the HtsA axial residues in the displacement.



In order to obtain the essential nutrient iron during infections, many bacterial pathogens acquire heme from their hosts using a combination of cell wall associated hemoreceptors and secreted hemophores.^{1–5} In many species of Gram-positive bacteria, captured heme is thought to be transferred across the cell wall via peptidoglycan hemoreceptors, which deliver the heme to specific membrane-associated ABC transporters^{6,7} that pump the heme into the cytoplasm.⁸ Significant advances have been made in understanding the heme acquisition pathways in a number of clinically important Gram-positive bacteria.^{5,9–11} Works have established the structural basis of heme binding for many hemoreceptors^{12–18} and established that heme transfer occurs rapidly via protein–protein heme transfer complexes.^{19–21} However, how heme is transferred from one protein to another in these processes is not well understood.

Our laboratory has been studying heme transfer from the surface heme-binding protein Shp to HtsA, the lipoprotein component of the ABC transporter HtsABC in Group A *Streptococcus* (GAS), as a model system to understand the mechanism of heme transfer among proteins.²² Shp and HtsABC are part of the heme acquisition machinery in GAS, which also includes the cell surface heme-binding protein Shr.^{23–26} Shr directly acquires heme from human methemoglobin and donates it to Shp.⁵ Heme can be directly transferred

from Shp to HtsA,¹⁹ but Shr does not efficiently donate its heme to HtsA.²⁶ These findings support a heme acquisition pathway by the Shr/Shp/HtsABC system in which Shr directly extracts heme from metHb and Shp relays it from Shr to HtsA (Figure 1). Although the specific proteins vary, similar heme transfer processes occur in other important pathogens, including *S. aureus* and *B. anthracis*.^{6,9,10,27}

Because the Shp to HtsA heme transfer reaction has been well defined, it is an ideal model system to understand the process of heme transfer in Gram-positive bacteria. Previously, we have shown that Shp and HtsA use the Met66/Met153 and Met79/His229 residues, respectively, as axial ligands to coordinate the central iron atom within bound heme.^{13,20,28} The heme complexes of each protein exhibit significantly different UV–vis absorption spectra, which makes it convenient to spectrally monitor the heme transfer reaction. In our previous work, we demonstrated that Met66Ala and Met153Ala mutations in Shp alter the kinetic mechanism through which heme is transferred to HtsA.²⁰ We also created HtsA axial ligand mutants and characterized how they coordinate heme iron.²⁸ Our previous kinetic analysis led us to hypothesize that

Received: July 18, 2013

Revised: August 25, 2013

Published: August 27, 2013



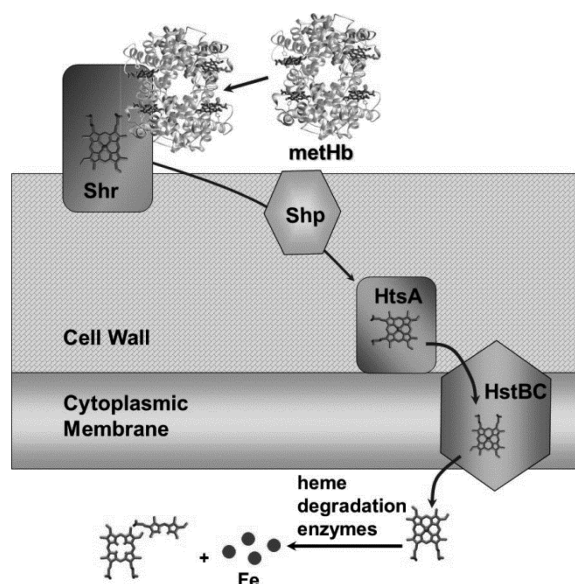


Figure 1. Scheme for the proposed model of heme acquisition from metHb by the Group A *Streptococcus* heme acquisition system consisting of the surface proteins Shr and Shp, lipoprotein HtsA, permease HtsB, and ATPase HtsC. The model is based on the findings in refs 5, 7, 19, and 23–26. The model was modified from that in ref 9.

heme-bound Shp (HoloShp) first forms a complex with heme-free HtsA (apoHtsA) and subsequently transfers its heme to HtsA with one kinetic phase.¹⁹ On the basis of this kinetic mechanism, we proposed that the axial residues of the Shp heme iron are directly displaced by the axial residues of apoHtsA during the heme transfer reaction. Here, we present data that support this proposed heme transfer mechanism.

MATERIALS AND METHODS

Proteins. Recombinant wild-type, Met66Ala (Shp^{M66A}) mutant, and Met153Ala (Shp^{M153A}) mutant Shp proteins and also wild-type, Met79Ala (HtsA^{M79A}) mutant, and His229Ala (HtsA^{H229A}) mutant HtsA proteins were prepared as previously described. Purified wild-type and M79A HtsA proteins were a mixture of holo and apo forms. Homogeneous apoHtsA proteins were obtained by loading the mixtures on a DEAE column (2.5 × 6 cm) and eluting the column with a 100 mL linear gradient of 0.05–0.15 M NaCl in Tris–HCl, pH 8.0.

Heme Transfer. Heme transfer from ferric holoShp to apoHtsA was monitored by spectral changes associated with heme transfer. Ferric holoShp, holoShp^{M66A}, or holoShp^{M153A} was mixed with wild-type, HtsA^{H229A}, or HtsA^{M79A} apoproteins at indicated concentrations in 20 mM Tris–HCl, pH 8, in a stopped-flow spectrophotometer equipped with a photodiode array detector (SX20; Applied Photophysics). Absorption spectra of each reaction mixture were recorded at different times after mixing.

Kinetic Analysis of Heme Transfer. Spectra of the heme transfer reactions were recorded with time using the stopped-flow spectrophotometer after mixing wild-type or mutant Shp with apoHtsA mutant protein at ≥ 5 X [holoShp protein] in 20 mM Tris–HCl, pH 8.0. Spectral changes at the Soret peak and the charge transfer bands were fit to a single exponential or double exponential equation using the GraphPad Prism Software, yielding observed pseudo-first order rate constants.

Magnetic Circular Dichroism (MCD) Measurements. MCD spectra of oxidized and reduced holoShp proteins in 50

mM phosphate buffer at the indicated pH were recorded using JASCO J-710 spectropolarimeter equipped with an Alpha Scientific 3002-1 electromagnet under the following conditions: bandwidth, 1 nm; accumulation, 3 scans; scan rate, 100 nm/min; resolution, 0.5 nm; magnetic field, 12.9 kG (1.29 T); temperature, 25 °C. The spectra of the reduced proteins were taken in the presence of excess dithionite. Buffer blank-corrected CD spectra obtained without the magnetic field were subtracted from corresponding buffer-corrected MCD spectra using the Jasco software. These processed MCD data were then used to calculate the final MCD data in units of $\Delta\epsilon_M$ (M cm T)^{−1} based on protein concentration, light path, magnetic field, and molar ellipticity Θ_M (deg cm² dmol^{−1} T^{−1}) = 3300 $\Delta\epsilon_M$.

Binding of Imidazole to Shp Mutant Proteins. One milliliter of 7 μ M Shp^{M66A} or Shp^{M153A} was mixed with imidazole at 5 to 500 μ M and incubated at 20 °C for at least 10 min, and the absorption and MCD spectra were recorded. The spectral change in the binding of imidazole to Shp^{M66A} versus imidazole concentration was analyzed using the model of specific one-site binding.

Other Assays and Measurements. Protein concentrations were measured using a modified Lowry protein assay kit (Pierce) with bovine serum albumin as a standard according to the manufacturer's instructions. Heme content of Shp and HtsA was determined using the pyridine hemochrome assay.²⁹ A SPECTRA^{max} 384 Plus spectrophotometer was used for absorption measurements, unless otherwise specified.

Structure Modeling and Docking. Modeler version 9.9^{30,31} was used to generate a three-dimensional (3-D) homology model of apoHtsA. Initially, Modeler was used to search a library containing the primary sequences of proteins of known structure. The top six related sequences that aligned to HtsA with 24% or greater sequence identity were used as templates to build a model of the three-dimensional structure of HtsA. The model of HtsA was then docked to holoShp (PDB ID: 2Q7A) using the online RosettaDock server.³² RosettaDock identifies low-energy conformations for the protein–protein complex by simultaneously optimizing side-chain conformations (packing algorithm) and through rigid body docking using a Monte Carlo minimization strategy.

RESULTS

Coordination of the Heme Iron in Shp^{M66A} and Shp^{M153A}. We hypothesize that transfer occurs when one of the axial ligands in Shp is displaced by a ligand from HtsA. We used HtsA^{M79A}, HtsA^{H229A}, Shp^{M153A}, and Shp^{M66A} mutants to test the hypothesis as described later. Information on the coordination and axial ligand(s) of the heme iron in these axial HtsA and Shp mutants is critical for the interpretation of spectral and kinetic data of the heme transfer reactions. UV–vis, MCD, RR, and EPR analyses have revealed that ferric HtsA^{H229A} has a high-spin pentacoordinate heme iron with a methionine axial ligand and that ferrous HtsA^{H229A} and HtsA^{M79A} heme irons are pentacoordinate, whereas ferric HtsA^{M79A} has a high-spin hexacoordinate heme iron with axial histidine and water ligands.²⁸ This left unresolved how potential heme coordinating ligand in axial Shp mutants interacted with iron. Thus, we examined the heme coordination in Shp^{M66A} and Shp^{M153A}. Resonance Raman analysis uses intense laser light for repeated excitation under which the wild-type Shp and axial mutant proteins form precipitates. Thus, we used MCD analysis to examine the heme coordination in the Shp mutant proteins. Ferrous wild-type Shp displays a typical

low-spin hexacoordinate heme iron in the Q-band region (Figure 2A); however, its Soret band has higher ellipticities and

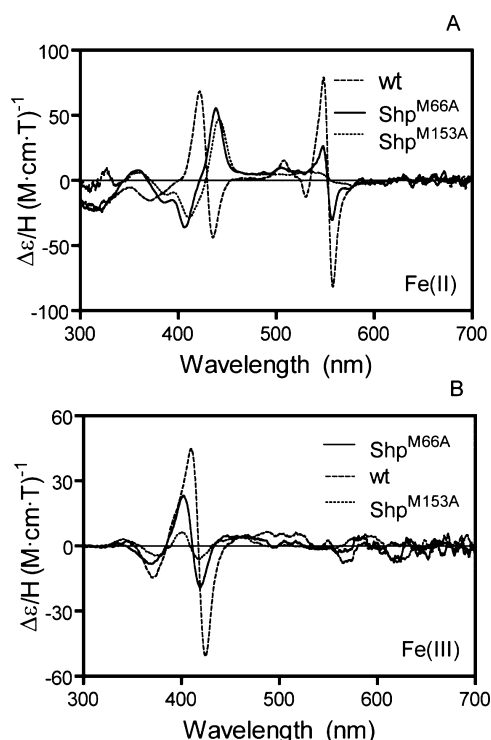


Figure 2. MCD Spectra of ferrous (A) and ferric (B) wild-type (wt), M66A, and M153A Shp in 20 mM Tris–HCl, pH 8.0. The reduced spectra were recorded in the presence of excess dithionite.

a higher red shift compared with the previously reported Soret band of HtsA with Met and His axial ligation.²⁸ The distinct MCD spectrum of ferrous Shp in the Soret band region is apparently due to the axial ligation of the iron to two Met residues, which has been elucidated by a mutagenesis study²⁰ and confirmed by the X-ray structure of the heme-binding domain of Shp.¹³ Ferrous Shp^{M153A} has an MCD profile (Figure 2A) that is very similar to that of ferrous HtsA^{H229A}, which has a pentacoordinate iron with an axial bond with Met79.²⁸ This result indicates that ferrous Shp^{M153A} has a pentacoordinate iron that bonds with the axial Met66 residue. Ferric wild-type Shp shows a typical hexacoordinate low-spin MCD spectrum (Figure 2B). The MCD spectrum of ferric Shp^{M153A} is, again, very similar to that of ferric HtsA^{H229A} (Figure 2B). The published UV–vis spectrum of ferrous and ferric Shp^{M153A}²⁰ is similar to that of ferrous and ferric HtsA^{H229A} (Table 1).²⁸ Thus, like HtsA^{H229A}, Shp^{M153A} has a pentacoordinate heme iron with a Met axial ligand (Met66).

Ferrous Shp^{M66A} and Shp^{M153A} share similar MCD profiles in the region of 350–450 nm, but Shp^{M66A} has a small derivative signal in the Q-band that is similar to that of the wild-type Shp (Figure 2A), suggesting that a small portion of ferrous Shp^{M66A} might be in a hexacoordinate complex. The MCD profile of ferric Shp^{M66A} is very similar to that of HtsA^{H229A} and Shp^{M153A}; however, the ellipticity of ferric Shp^{M66A} at the Soret band at pH 8.0 is about three times those of HtsA^{H229A} and Shp^{M153A}. According to the results of a pH titration described later, the higher ellipticities of Shp^{M66A} at pH 8.0 appear to be partly due to the presence of a small portion of Shp^{M66A} that has a hexacoordinate heme iron with a water molecule at the vacated coordination site.

Table 1. Heme Coordination and Spectral Features of Wild-type and Mutant HtsA Proteins

protein ^a	known/proposed axial ligand(s)	absorption peaks			major MCD features			
		Soret (nm)	ϵ (mM ^{−1} cm ^{−1})	visible (nm)	Soret (nm)	$\Delta\epsilon/H$ (M cm T ^{−1})	visible (nm)	$\Delta\epsilon/H$ (M cm T ^{−1})
Shp	Met/Met	420	116	529 560	410 417 424	44.8 0 −50.9	550 554 564	2.7 0 −7.8
Shp ^{M66A} (pH 9.0)	Met	404	120	486 528 604	403 412 418	17.3 0 −12.3	583 601 618	4.6 0 −9.2
Shp ^{M66A} (pH 8.0)	Met and Met/H ₂ O ^a	406	128	490 526 601	403 411 419	26.1 0 −18.6	592 603 620	3.7 0 −6.7
Shp ^{M66A} (pH 6.0)	Met/H ₂ O	408	157	502 624	403 410 417	34.2 0 −26	620 627 632	−1.3 −2.1 −3.5
Shp ^{M153}	Met	402	100	480 ^b 598	401 409 418	6.4 0 −6.3	588 607 624	5.2 0 −7.4
HtsA ^c	Met/His	412	123	532 562 ^b	407 416 423	38 0 −45	557 564 578	1.9 0 −5.6
HtsA ^{M79A,c}	His/H ₂ O	403	187	498 536 ^b 630	399 407 414	20 0 −16.5	548 580 643	−1.5 −2 −3.3
HtsA ^{H229A,c}	Met	402	114	482 524 600	404 410 419	11 0 −7.5	589 608 624	4.9 0 −7.2

^aAll spectra were measured at pH 8.0 unless specified. ^bEstimated from shoulders. ^cData for HtsA proteins are from ref 28.

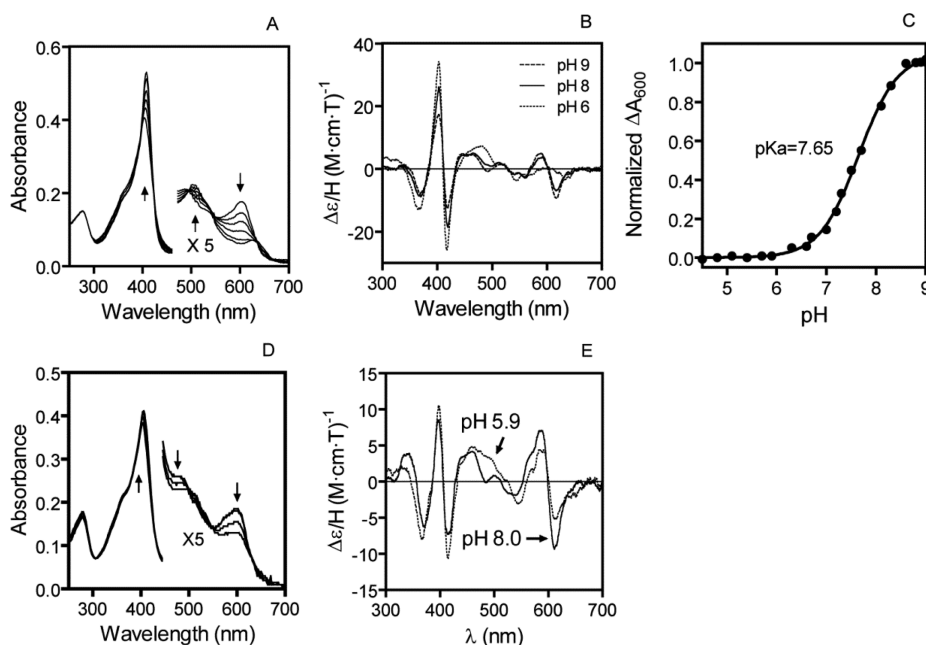


Figure 3. Effect of pH on optical and MCD spectra of Shp^{M66A} and Shp^{M153A}. (A) Spectral shift of Shp^{M66A} as a function of pH. pH values: 9.0, 8.1, 7.7, 7.3, 6.7, 5.9. (B) MCD spectra of Shp^{M66A} at the indicated pH. (C) pH titration curve of A_{600} of Shp^{M66A}. (D and E) Optical and MCD spectra of Shp^{M153A} at pH 8.1, 7.3, 6.4, and 5.9. The arrows indicate the direction of the shift as pH decreased.

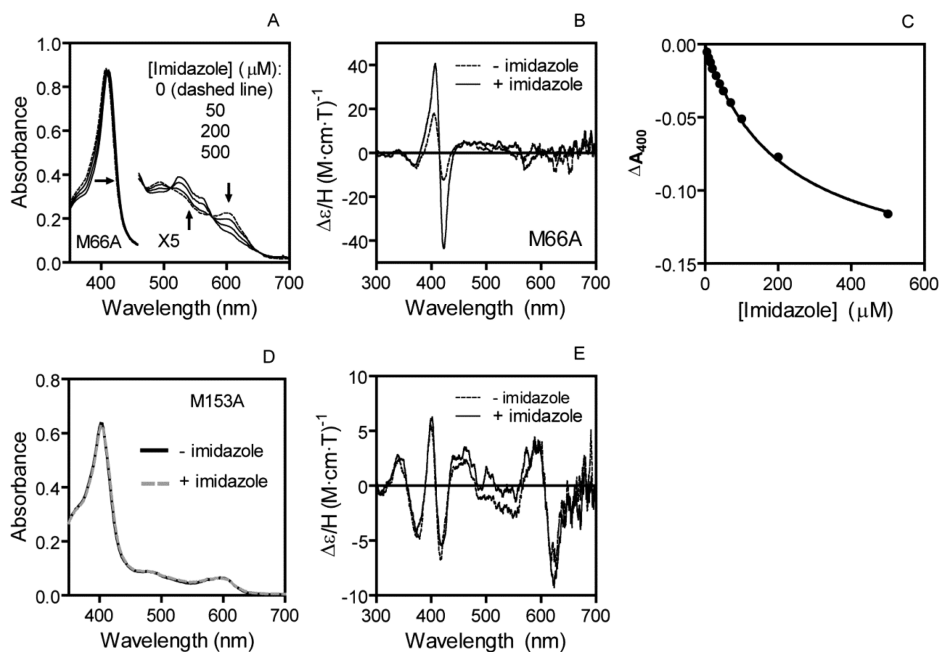


Figure 4. Effects of imidazole on optical (A and D) and MCD (B and E) spectra of Shp^{M66A} and Shp^{M153A}. The optical and MCD spectra of each Shp protein in 20 mM Tris–HCl (for optical spectra) or 50 mM potassium phosphate (for MCD), pH 8.0, at the indicated imidazole concentrations. The arrows in panel A indicate the directions of the spectral shifts as imidazole concentration changes. (C) Imidazole titration of ΔA_{400} of Shp^{M66A}.

Effects of pH on the Coordination of the Heme Iron in Shp^{M66A}. The UV–vis spectrum of ferric Shp^{M66A} varied from pH >8.6 to pH 6.0. At pH >8.6, ferric Shp^{M66A} displayed absorption peaks at 404, 489, and 600 nm (Figure 3A). This spectrum is similar to that of both Shp^{M153A} and HtsA^{H229A} and, thus, represents a pentacoordinate heme iron complex with one axial bond to Met153. As the pH decreases from pH 8.6 to ≤6, the Soret absorption peak increases in intensity and is red-shifted. The charge transfer bands in the visible region undergo dramatic changes as well, resulting in an absorption spectrum

with peaks at 408, 502, 534, and 624 nm at pH 6 (Figure 3A). This spectrum resembles that of a hexacoordinate high-spin heme iron with its sixth bond to an axial water molecule, suggesting that Shp^{M66A} had a switch in the heme iron coordination from pentacoordination to hexacoordination due to the binding of a water molecule as the sixth coordination. MCD measurements support this interpretation. The MCD spectra of ferric Shp^{M66A} at basic and acidic pH are similar to those of the pentacoordinate HtsA^{H229A} complex and the hexacoordinate heme complex, respectively (Figure 3B). The

spectral changes of ferric Shp^{M66A} with pH fit an equation describing the absorbance change with the titration of a single ionizable group with a pK_a of 7.6 ± 0.1 (Figure 3C), indicating that the conversion of the heme iron coordination in Shp^{M66A} is associated with the protonation of a basic group. The UV-vis spectrum of ferric Shp^{M153A} did not change as dramatically as that of ferric Shp^{M66A} (Figure 3D). Consistent with this observation, the MCD spectrum of Shp^{M153A} at pH 6.0 was still very similar to that of the protein at pH 8.0, indicating that the majority of the heme iron does not change the coordination when pH decreases from 8.0 to 6.0 (Figure 3E).

Binding of Imidazole to the Heme Iron in Axial Mutants of Shp. The pH titration results suggest that the empty coordination site in Shp^{M66A} and Shp^{M153A} have different accessibility to external ligands. The understanding of the accessibility would provide clues about the axial displacement process. To investigate this issue, we tested the ability of Shp^{M66A} and Shp^{M153A} to interact with free imidazole, which was meant to act as a surrogate for HtsA. The addition of imidazole causes a dose-dependent shift of the Shp^{M66A} absorption spectrum to one that is typical of a hexacoordinate low-spin heme iron (Figure 4A), and the MCD spectrum of Shp^{M66A} in the presence of 0.5 mM imidazole is consistent with the imidazole binding (Figure 4B). The spectral change as a function of imidazole concentration fit a model of specific one-site binding with a K_d of $210 \pm 11 \mu\text{M}$ (Figure 4B). These results indicate that imidazole ligates to the Shp^{M66A} heme iron. In contrast, imidazole at 0.5 mM did not alter the absorption and MCD spectra of Shp^{M153A} (Figure 4C,D), indicating that imidazole cannot bind to Shp^{M153A} under these conditions. These results suggest that imidazole can access the alanine 66 position of Shp^{M66A} but not the alanine 153 position of Shp^{M153A}.

Effects of Mutation of the HtsA Heme Axial Ligand Residues on Heme Transfer from Shp to HtsA and its Kinetic Mechanism. The purpose of this study is to probe the mechanism of heme transfer from Shp to HtsA by using Shp and HtsA heme axial residue mutants. With the information on the spectral features and coordination of the heme iron in the axial Shp and HtsA mutants, we could interpret the heme transfer according to spectral changes during the heme transfer reaction and determine the mechanism of heme transfer by monitoring the kinetics of the spectral changes associated with heme transfer. We first examined the effects of the Ala replacements of the HtsA heme axial ligands on the efficiency and the kinetic feature of the Shp-to-HtsA heme transfer. In the reaction of ferric Shp and apoHtsA^{M79A}, the Soret peak shifts rapidly from 420 to 402 nm with a concurrent decrease of the charge transfer bands at 530 and 560 nm, and an additional peak at 630 nm appeared (Figure 5A). The resulting spectrum has peaks at 402, 498, 536, and 630 nm. This spectrum is the same as the reported spectrum of holoHtsA^{M79A}.²⁸ Thus, ferric Shp efficiently transfers its heme to HtsA^{M79A}. However, there was no significant spectral shift after ferric Shp was mixed with excess apoHtsA^{H229A}, and the final spectrum of the mixture was primarily that of holoShp but not holoHtsA^{H229A} (Figure 5B), indicating that most of the heme was still on Shp. Thus, elimination of the His229 ligand, but not the Met79 residue, considerably decreases the efficiency of heme transfer from ferric holoShp to apoHtsA.

Next, we determined whether the HtsA^{M79A} mutation changes the kinetic mechanism of the Shp/apoHtsA reaction. We monitored spectral changes of the Soret peak at A_{402} and

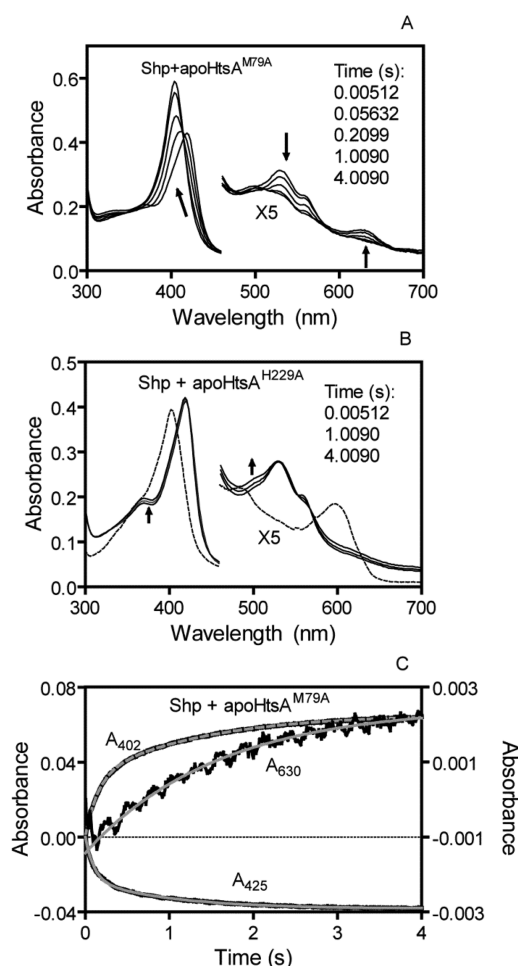


Figure 5. Spectral and kinetic analyses of heme transfer from ferric holoShp to apoHtsA^{M79A} and apoHtsA^{H229A}. (A) Shifts of the absorption spectrum in the reaction of $3.5 \mu\text{M}$ ferric holoShp with $30 \mu\text{M}$ apoHtsA^{M79A} in 20 mM Tris-HCl, pH 8.0, at room temperature after mixing in a stopped-flow spectrophotometer. The arrows indicate the directions of the spectral shifts with time. (B) Absorption spectra of the reaction mixture of $3.5 \mu\text{M}$ ferric holoShp with $30 \mu\text{M}$ apoHtsA^{H229A} at the indicated time points after mixing. The spectrum of $3.5 \mu\text{M}$ holoHtsA^{H229A} (gray line) is included for comparison. (C) Time course of ΔA_{402} and ΔA_{425} at the Soret peak and ΔA_{630} at the charge transfer bands in the holoShp/apoHtsA^{M79A} reaction as in panel A. The black traces and gray curves represent the observed data and double (for ΔA_{402} and ΔA_{425}) or single (for ΔA_{630}) exponential fitting curves, respectively.

A_{425} and the charge transfer band at A_{630} . ΔA_{402} and ΔA_{425} increased and decreased with time, respectively, representing the formation of holoHtsA^{M79A} and disappearance of holoShp, respectively. The time courses of both ΔA_{402} and ΔA_{425} fit to a double exponential equation (Figure 5C), resulting in observed rate constants of 7.4 ± 0.10 and $0.65 \pm 0.02 \text{ s}^{-1}$ from the ΔA_{402} time course and 7.6 ± 0.12 and $0.70 \pm 0.03 \text{ s}^{-1}$ for the ΔA_{425} time course with $32 \mu\text{M}$ of apoHtsA^{M79A} (Table 2). There was not much change in ΔA_{630} in the fast phase, and the ΔA_{630} time course for the slower phase fits a single exponential equation, yielding an observed rate constant of $0.63 \pm 0.03 \text{ s}^{-1}$. This observed rate was similar to the one for the second kinetic phase in the ΔA_{402} and ΔA_{425} time courses. The A_{630} peak is the absorption of holoHtsA^{M79A}. Thus, the final product was completely formed during the second kinetic phase. Thus, like the M66A and M153A mutations of Shp, the M79A mutation

Table 2. Number of Kinetic Phase and Rate Constants in Heme Transfer from Shp Proteins to HtsA Proteins

donor	acceptor	no. of kinetic phase	k_t (s ⁻¹)	k_{t_1} (s ⁻¹)	k_{t_2} (s ⁻¹)	reference
Shp	HtsA	1	43 ± 3			19
Shp	HtsA ^{M79A}	2		7.4 ^a	0.8 ^a	this work
Shp	HtsA ^{H229A}	no transfer				this work
Shp ^{M66A}	HtsA	2		8.7 ± 0.3	0.38 ± 0.08	20
Shp ^{M66A}	HtsA ^{M79A}	1	8.6 ± 0.6 ^b			this work
Shp ^{M66A}	HtsA ^{H229A}	2		7.0 ± 1.0 ^c	1.4 ± 0.5 ^c	this work
Shp ^{M153A}	HtsA	2		120 ± 30	2.5 ± 0.2	20
Shp ^{M153A}	HtsA ^{M79A}	2		8.1 ± 0.4 ^b	0.48 ± 0.06 ^b	this work
Shp ^{M153A}	HtsA ^{H229A}	1	14.7 ± 0.3 ^c			this work

^aApparent rate constant obtained at 32 μM apoHtsA^{M79A}. ^bApparent rate constant obtained at 10 μM apoHtsA^{M79A}. ^cApparent rate constant obtained at 13 μM apoHtsA^{H229A}.

of HtsA results in a change in the kinetic mechanism from one to two kinetic phases. It should be noted that the biphasic kinetics of the holoShp/apoHtsA^{M79A} is more related to the cleavage of the axial bonds in the heme donor, whereas the biphasic features of the Shp axial mutant/apoHtsA is more related to the formation of the axial bonds in the holoHtsA product.

Model for Axial Ligand Replacement Mechanism in the Shp-to-HtsA Heme Transfer Reaction. The heme transfer reaction involves the cleavage of the two axial bonds of the Shp heme and the formation of the two new axial bonds of the heme in the holoHtsA product. The single kinetic phase of this transfer reaction indicates that the cleavage of the Shp heme axial bonds and the formation of the HtsA heme axial bonds occur at about the same time. We propose that the axial residues of apoHtsA approach the axial bonds along the two sides of the heme in Shp to facilitate the cleavage of the axial bonds and eventually displace the Shp axial residues at about same time (Figure 6A). The evidence for the specific displacements of the Shp M66 and M153 axial ligands with HtsA M79 and His229, respectively, in this model is presented below. The kinetic mechanism of the Shp/apoHtsA^{M79A} reaction is consistent with and, thus, supports the reaction model in Figure 6A. The fast phase in the Shp/apoHtsA^{M79A} reaction represents the displacement of the Shp M153-heme iron bond with the HtsA H229 residue, and the slower phase is the cleavage of the Shp M66-heme iron bond because of the lack of the HtsA M79 residue (Figure 6B).

Test on the Axial Ligand Displacement Model for the Heme Transfer from Shp to HtsA. The axial displacement model in Figure 6A can be tested by examining heme transfer from Shp^{M66A} and Shp^{M153A} to apoHtsA^{M79A} and apoHtsA^{H229A}. If the remaining axial residue in the HtsA mutants displaces the remaining axial residue in the Shp mutants, the transfer process should have one kinetic phase (Figure 6C). Otherwise, the reaction should be kinetically biphasic (Figure 6D). In particular, there should be a hexacoordinate intermediate in the transfer reaction in Figure 6D.

In the reactions of apoHtsA^{H229A} with holoShp^{M66A} and holoShp^{M153A}, the donors and product all have a pentacoordinate heme iron with a Met axial ligand and have a charge transfer absorption peak at about 600 nm. During the reaction of holoShp^{M66A} with apoHtsA^{H229A}, the Soret peak first has a red shift and then a blue shift (Figure 7A), and the A₆₀₀ peak first decreases (the black curves) and then increases (the colored curves) (Figure 7A). ΔA₄₂₀ that represents the spectral shift in the Soret peak first increases and then decreases, whereas ΔA₆₀₀ shows the spectral shift in the charge transfer

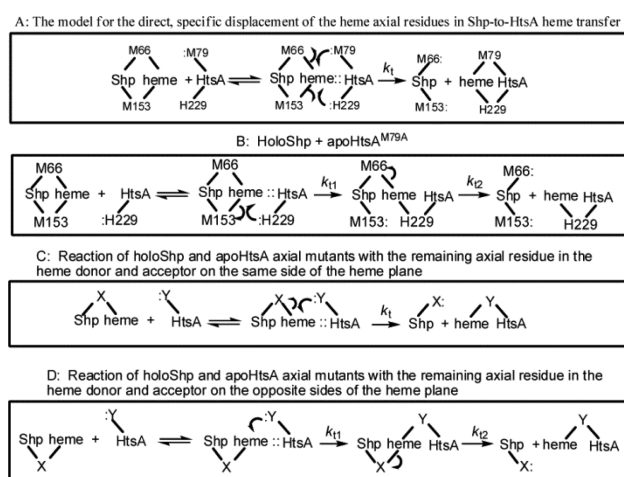


Figure 6. Proposed schemes for the reactions among the wild-type and axial mutant proteins of holoShp and apoHtsA. M66/M153 and M79/H229 are the axial ligand residues in Shp and HtsA, respectively, and are also represented by X and Y when their identity and relative locations cannot be specified. The short lines to heme represent the axial bonds to the heme iron. (A) Model for the Shp-to-HtsA heme transfer in which the Met66 and M153 axial residues of holoShp are specifically displaced by the Met79 and His229 residues of apoHtsA, respectively. (B) Reaction scheme for the kinetically biphasic ferric holoShp/apoHtsA^{M79A} reaction. Kinetically single-phase (C) and biphasic (D) reactions of ferric holoShp axial mutants with apoHtsA axial mutants.

band first decreases and then increases (Figure 7B). The time course of both ΔA₄₂₀ and ΔA₆₀₀ at 13 μM of apoHtsA^{H229A} fit to a double exponential equation, yielding two observed rate constants of 7.0 ± 1.0 and 1.4 ± 0.5 s⁻¹. Clearly, the holoShp^{M66A}/apoHtsA^{H229A} reaction has an intermediate. The Soret peak of this intermediate is at a longer wavelength than holoShp^{M66A} and holoHtsA^{H229A}, and the intermediate lacks the A₆₀₀ peak. These features suggest that the intermediate in the holoShp^{M66A}/apoHtsA^{H229A} reaction is a hexacoordinate heme iron complex. These results suggest that the holoShp^{M66A}/apoHtsA^{H229A} reaction follows the reaction scheme shown in Figure 5D, in which the Met79 residue of apoHtsA^{H229A} first forms an axial bond with the heme iron prior to the cleavage of the Met153–Fe bond during the reaction.

In contrast, there is no significant change in A₆₀₀ during the reaction of holoShp^{M153A} with apoHtsA^{H229A} (Figure 7C,D), and the Soret peak increased with time (Figure 7C). The time course of ΔA₄₁₀ fits to a single exponential equation (Figure 4D), yielding an observed rate constant of 14.7 ± 0.3 s⁻¹ at 13

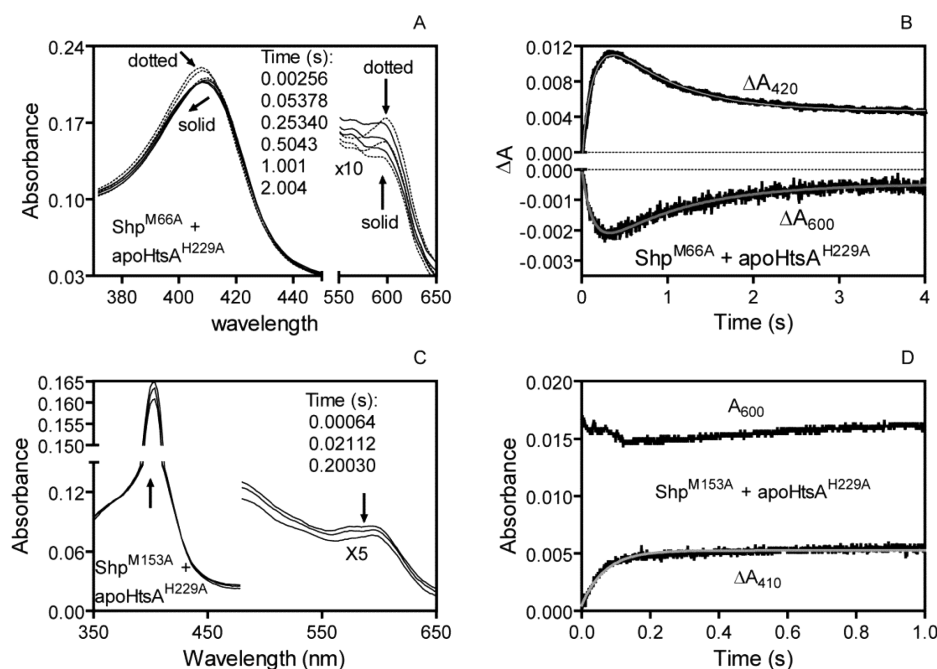


Figure 7. Transfer intermediate in ferric holoShp^{M66A}/apoHtsA^{H229A} reaction, but not in the holoShp^{M153A}/apoHtsA^{H229A} reaction. HoloShp mutant was mixed with apoHtsA mutant in 20 mM Tris–HCl in a stopped-flow spectrophotometer. The arrows indicate the direction of the spectral shift with time. (A) Spectral shift in the reaction of 1.2 μ M holoShp^{M66A} with 13 μ M apoHtsA^{H229A}. The dotted and solid curves are in the initial fast and subsequent slow phases, respectively. (B) Time course of ΔA_{420} and ΔA_{600} for the reaction in panel A. The black traces and gray curves represent the observed data and double exponential fitting curves, respectively. (C) Spectral shift in the reaction of 0.9 μ M holoShp^{M153A} with 13 μ M apoHtsA^{H229A}. (D) Time course of ΔA_{410} and ΔA_{600} for the reaction in panel C. The black traces represent the observed data, and the gray curve of ΔA_{410} is the single exponential fitting curve.

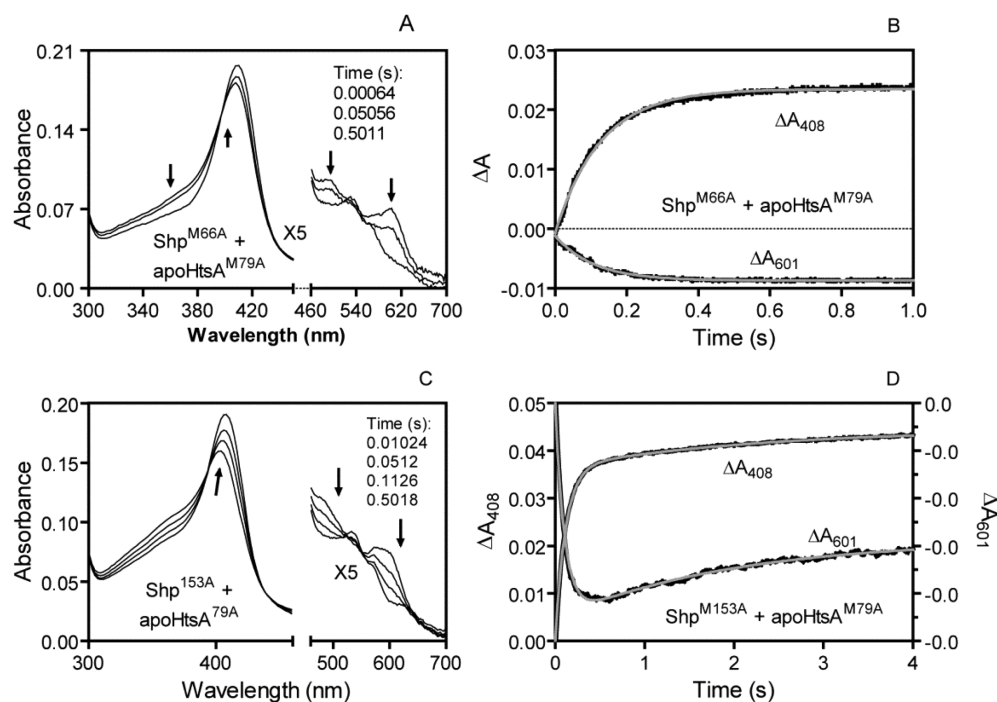


Figure 8. Different kinetic phases of the heme transfer reactions of apoHtsA^{M79A} with ferric holoShp^{M66A} and holoShp^{M153A}. HoloShp mutant (0.9 μ M) was mixed with 10 μ M apoHtsA mutant in 20 mM Tris–HCl in a stopped-flow spectrophotometer. The arrows indicate the orientation of the spectral shift with time. (A) Spectral shift in the reaction of holoShp^{M66A} with apoHtsA^{M79A}. (B) Single-phase time course of ΔA_{418} and ΔA_{600} for the reaction in panel A. The black traces and gray curves represent the observed data and single exponential fitting curves, respectively. (C) Spectral shift in the reaction of holoShp^{M153A} with apoHtsA^{M79A}. (D) Kinetically biphasic time course of ΔA_{408} and ΔA_{601} for the reaction in panel C. The black traces and gray curves represent the observed data and double exponential fitting curves, respectively.

μM apoHtsA^{H229A}. Thus, the holoShp^{M153A}/apoHtsA^{H229A} reaction has one kinetic phase, indicating that there is no spectrally detectable intermediate in this reaction. This spectral and kinetic data can be interpreted by the scheme shown in Figure 6C, in which the HtsA M79 residue displaces the Shp M66 residue. The results in the reactions of apoHtsA^{H229A} with Shp^{M66A} and Shp^{M153A} support a mechanism of the specific axial residue displacement shown in Figure 6A, in which the Met66 and Met153 residues of Shp are specifically displaced by the Met79 and His229 residues of apoHtsA, respectively, during the reaction.

This axial displacement model was further tested in the reactions of apoHtsA^{M79A} with holoShp^{M66A} and holoShp^{M153A}. If this model is correct, the holoShp^{M66A}/apoHtsA^{M79A} reaction should follow the scheme shown in Figure 6C and have one kinetic phase, whereas the Shp^{M153A}/apoHtsA^{M79A} reactions should have follow the scheme shown in Figure 6D and have two kinetic phases. In both reactions, the spectra shifted to that of holoHtsA^{M79A} (Figure 8A,C). The spectral change in the holoShp^{M66A}/apoHtsA^{M79A} reaction indeed fits to a single exponential equation with an observed rate constant of $8.6 \pm 0.6 \text{ s}^{-1}$ with $10 \mu\text{M}$ apoHtsA^{M79A} (Figure 8B), indicating one kinetic phase of the reaction, whereas the spectral change in the holoShp^{M153A}/apoHtsA^{M79A} reaction fits to a double exponential equation with observed rate constants of $8.1 \pm 0.4 \text{ s}^{-1}$ and $0.48 \pm 0.06 \text{ s}^{-1}$ with $10 \mu\text{M}$ of apoHtsA^{M79A}. These results further support the specific displacement of the axial ligands of the heme iron during the Shp-to-HtsA heme transfer reaction as proposed in Figure 5A.

Juxtaposition of the Shp and HtsA Heme-Binding Sites in Structural Modeling and Docking. To further examine the mechanism of the specific axial displacement in the Shp/HtsA reaction shown in Figure 6A, we used structural modeling and docking to examine whether the heme-binding pocket in Shp and HtsA can be juxtaposed in a way that is consistent with the model in Figure 6A. The X-ray crystal structure of the heme-binding domain of Shp is available¹³ but the structure of HtsA is not. We first generated a 3-D homology model of apoHtsA using the Modeler program,^{30,31} which is very similar to the structure of IsdE,³³ a homologue of HtsA. The apoHtsA model was then docked to the structure of the heme-binding domain of Shp (PDB ID: 2Q7A) using the online RosettaDock server.³² Although many possible protein orientations were obtained from the docking exercise, in many of the low-energy complexes, the proteins were orientated as shown in Figure 9. Thus, the docking analysis results are

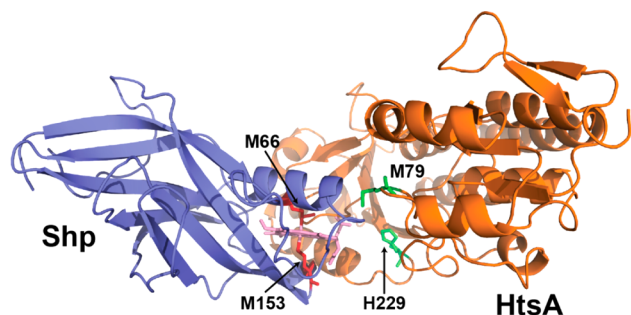


Figure 9. Docking complex with the juxtaposed heme pockets of Shp and lowest energy. Structure elements: blue, Shp protein; orange, HtsA protein; light pink, heme; red, the M66 and M153 axial residues in Shp; green, the M79 and H229 axial residues.

compatible with the axial displacement heme transfer mechanism we have formulated in which HtsA His229-for-Shp M153 and HtsA M79-for-Shp M66 displacements occur.

DISCUSSION

This study presents evidence for a novel mechanism of heme transfer from one protein to another. We first characterized the coordination and external ligand accessibility of the heme iron in the axial mutants of Shp for the interpretation of the spectral change and kinetics of heme transfer from the Shp axial ligand mutants to HtsA axial ligand mutants. We then revealed the roles of the axial residues of the HtsA heme iron in the efficiency and kinetic mechanism of the Shp-to-HtsA heme transfer. The H229 and M79 residues of HtsA are essential for the efficiency and single kinetic phase mechanism of the heme transfer from ferric Shp to HtsA, respectively. Finally, this study elucidated the mechanism of the specific displacement of the axial residues in the Shp/HtsA heme transfer reaction. The axial residues M66 and M153 of Shp are displaced by the axial residues M79 and H229 of HtsA, respectively, during the holoShp/apoHtsA reaction. These findings provide novel insight into the mechanism of direct heme transfer from one protein to another.

A novel advancement of this study is the elucidation of the specific displacement of the axial residues of Shp and HtsA during their reaction; that is, the Met66 and Met153 residues of Shp are specifically displaced by the Met79 and His229 residues of apoHtsA, respectively, during the heme transfer reaction. The spectral characterization on the coordination of the Shp^{M66A} and Shp^{M153A} heme iron together with that of HtsA^{M79A} and HtsA^{H229A} provides critical information for the interpretation of the heme transfer data using the Shp and HtsA mutants. The pentacoordinate heme iron of HtsA^{H229A} has an absorption peak at $\sim 600 \text{ nm}$,²⁸ which is also observed in a H102 M mutant of cytochrome b562 with an axial Met ligand.³⁴ Shp^{M66A} at basic pH and Shp^{M153} show optical and MCD spectra similar to that of HtsA^{H229A}, indicating the pentacoordination of the heme iron with the axial Met ligation in these mutants. Bonding to a water molecule at the empty sixth coordination site of Shp^{M66A} abolishes the A_{600} peak. The A_{600} peak-related spectral changes in the holoShp^{M66A}/apoHtsA^{H229A} and holoShp^{M153A}/apoHtsA^{H229A} reactions are consistent with the interpretation that the Met79 residue of apoHtsA^{H229A} forms the axial bond on the axial bond-lacking side of the pentacoordinate Shp^{M66A} heme, resulting in a hexacoordinate complex in the holoShp^{M66A}/apoHtsA^{H229A} reaction, and that the Met79 residue of apoHtsA^{H229A} directly replaces the Met66 residue in the holoShp^{M153A}/apoHtsA^{H229A} reaction, lacking a hexacoordinate heme transfer intermediate. Thus, the HtsA Met79 residue replaces the Shp Met66 residue. The kinetic analysis of the heme transfer in the holoShp^{M66A}/apoHtsA^{H229A} and holoShp^{M153A}/apoHtsA^{H229A} reactions confirms this conclusion. Furthermore, the kinetic mechanisms of the reactions of apoHtsA^{M79A} with holoShp^{M66A} and holoShp^{M153A} indicate that the His229 residue of HtsA forms the axial bond on the Met153 side of the Shp heme. The docking analysis supports the specific axial ligand displacement mechanism. These new data add more details to the “plug-in” model of the Shp/HtsA reaction, which was proposed to interpret the single kinetic phase of the Shp-to-HtsA heme transfer reaction.¹⁹ The updated model can be described in Figure 6A, where the empty heme pocket of apoHtsA slides in along the two sides of the bound heme in Shp in such a way

that the Met79 and His229 residues in apoHtsA are in close proximity of the Met66– and Met153–iron bonds in Shp, respectively, to displace the axial residues of Shp at about same time and pull it into the heme binding pocket of HtsA.

According to this specific displacement of the axial ligands of the Shp heme iron by the axial ligands of heme in HtsA, the rate constants for the cleavage rates of the Shp Met66–Fe bond in the reactions of apoHtsA^{M79A} with holoShp and holoShp^{M153A} were only about 5% of the cleavage of the Met66–Fe bond in the presence of the Met79 residue in the holoShp^{M153A}/apoHtsA^{H229A} reaction. The rate constant of the cleavage of the Met153–Fe bond in the presence of the His229 residue in the Shp^{M66A}/apoHtsA^{M79A} reaction was four times that of the Met153–Fe bond cleavage in the absence of the His229 residue in the holoShp^{M66A}/apoHtsA^{H229A} reaction. Thus, the axial ligand residues of the heme acceptor apoHtsA facilitate the cleavage of the axial bonds in holoShp. The two kinetic phases of the holoShp/apoHtsA^{M79A} further support the role of the axial residues of the HtsA heme iron in the cleavage of the axial bonds of heme in Shp. In this reaction, the cleavage of the Met153–Fe bond in Shp is facilitated by the HtsA His229 residue, whereas the cleavage of the other axial bond in Shp is slower because Met79 is absent. Thus, the axial residues of HtsA are actively involved in the specific displacement of the axial residues of the Shp heme iron. This work may help explain how the other NEAT-containing protein-to-lipoprotein transfer reactions occur as well.

How heme is transferred from one protein to another is not fully understood. Structural studies reveal transient IsdA/IsdC³⁵ and IsdC/IsdE³⁶ complexes and a stable HasA/HasR³⁷ complex, and the heme pockets of the donor and acceptor in both the reactions are juxtaposed. A docking analysis of the HasA/HasR interaction suggests that the interaction causes one of the two axial heme coordinations of HasA to break, and a subsequent steric displacement of heme by a receptor residue ruptures the other axial coordination.³⁷ Kinetic analyses of the Shp/HtsA and IsdA/IsdC reactions indicate the existence of an activated donor–acceptor complex.^{19,21} These studies support a direct heme transfer mechanism. Pilpa et al. proposed a release and capture mechanism for heme transfer from methHb to IsdH or IsdB in which donor/acceptor interaction enhances heme release from the donor, and released heme is then scavenged by the acceptor.¹⁷ This release/capture mechanism may be true for the methHb/IsdH reaction.³⁸ Our work provides further insight into the heme transfer mechanisms. First, the two axial ligands in the heme acceptor specifically displace the axial ligands in the donor. Second, the accepting axial ligands play a role in facilitating the cleavage of the axial bond in the donor. This specific displacement of axial ligands may occur in other heme acquisition systems. The heme iron in both IsdA and IsdC has a pentacoordination with a Tyr ligation, and the IsdA-to-IsdC heme transfer displays a single kinetic phase,²¹ suggesting that the axial Tyr residue in IsdC displaces the axial Tyr residue in IsdA.

It is known that the axial ligands of the heme iron in HasA, HasR, ShuA, and *Porphyromonas gingivalis* heme receptor HmuR are critical for heme transfer and acquisition.^{1,2,39–42} However, it is unclear why these axial ligands are required for heme acquisition. The earlier discussion suggests an active role of the axial residues in the heme acceptor in the heme transfer reaction. The inability of HtsA^{H229A} to acquire heme from ferric Shp indicates another role of the axial ligands of the heme recipient in driving the reaction equilibrium to the formation of

the transfer product. The H229A replacement of HtsA reduced the affinity of HtsA for heme.²⁸ The reduction in the heme affinity of HtsA^{H229A} mutant could be a primary reason why HtsA^{H229A} cannot efficiently acquire heme from ferric Shp. This interpretation is supported by the observations that the M79A replacement did not dramatically affect the heme affinity of HtsA²⁸ and that HtsA^{M79A} can efficiently take up heme from ferric Shp. Thus, the axial ligand of the heme acceptor can drive the equilibrium of the transfer reaction by enhancing the heme affinity of the acceptor.

It is interesting that only one axial ligand is critical to the affinity of HtsA for heme. This phenomenon is not limited to HtsA. The axial ligand residue of Shp, Met153, is critical to the high affinity of Shp for heme, whereas the other axial ligand residue, Met66, destabilizes heme binding.²⁰ These observations are consistent with the fact that *S. aureus* IsdA, IsdC, and IsdH and *B. anthracis* IsdX2 contain a pentacoordinate heme with tyrosine as the only axial ligand.^{12,14–16,43} Therefore, it appears that only one axial ligand of the heme iron is critical for high affinity of hemoproteins for heme.

AUTHOR INFORMATION

Corresponding Author

*B. Lei. E-mail: blei@montana.edu. Tel: (406) 994-6389. Fax: (406) 994-4303.

Present Address

[§]Y. Ran. Department of Cell Biology, University of Pittsburgh, School of Medicine, Pittsburgh, Pennsylvania 15261.

Funding

This work was supported in part by National Institutes of Health grants AI095704 (B.L.), AI097703 (B.L.) and AI52217 (R.T.C.) from the National Institute of Allergy and Infectious Diseases and GM103500-09 from the National Institute of General Medical Sciences, U.S. Department of Agriculture Formula Fund, and the Montana State University Agricultural Experimental Station.

Notes

The authors declare no competing financial interest.

ABBREVIATIONS

Shp, surface heme-binding protein; HtsA, lipoprotein component of the heme-specific ATP-binding cassette transporter; Shp^{M66A} and Shp^{M153A}, Shp mutants carrying alanine replacement of the axial Met66 and Met153 residues, respectively; HtsAM79A and HtsAH229A, HtsA mutants carrying alanine replacement of the axial Met79 and His229 residues, respectively

REFERENCES

- (1) Izadi-Pruneyre, N., Huche, F., Lukat-Rodgers, G. S., Lecroisey, A., Gilli, R., Rodgers, K. R., Wandersman, C., and Delepelaire, P. (2006) The heme transfer from the soluble HasA hemophore to its membrane-bound receptor HasR is driven by protein-protein interaction from a high to a lower affinity binding site. *J. Biol. Chem.* 281, 25541–25550.
- (2) Burkhard, K. A., and Wilks, A. (2007) Characterization of the outer membrane receptor ShuA from the heme uptake system of *Shigella dysenteriae*. Substrate specificity and identification of the heme protein ligands. *J. Biol. Chem.* 282, 15126–15136.
- (3) Fabian, M., Solomaha, E., Olson, J. S., and Maresso, A. W. (2009) Heme transfer to the bacterial cell envelope occurs via a secreted hemophore in the Gram-positive pathogen *Bacillus anthracis*. *J. Biol. Chem.* 284, 32138–32146.

- (4) Torres, V. J., Pishchany, G., Humayun, M., Schneewind, O., and Skaar, E. P. (2006) Staphylococcus aureus IsdB is a hemoglobin receptor required for heme iron utilization. *J. Bacteriol.* 188, 8421–8429.
- (5) Lu, C., Xie, G., Liu, M., Zhu, H., and Lei, B. (2012) Direct heme transfer reactions in the Group A Streptococcus heme acquisition pathway. *PLoS One* 7, e37556.
- (6) Mazmanian, S. K., Skaar, E. P., Gaspar, A. H., Humayun, M., Gornicki, P., Jelenska, J., Joachmiak, A., Missiakas, D. M., and Schneewind, O. (2003) Passage of heme-iron across the envelope of Staphylococcus aureus. *Science* 299, 906–909.
- (7) Liu, M., and Lei, B. (2005) Heme transfer from streptococcal cell surface protein Shp to HtsA of transporter HtsABC. *Infect. Immun.* 73, 5086–5092.
- (8) Drazek, E. S., Hammack, C. A., and Schmitt, M. P. (2000) Corynebacterium diphtheriae genes required for acquisition of iron from haemin and haemoglobin are homologous to ABC haemin transporters. *Mol. Microbiol.* 36, 68–84.
- (9) Zhu, H., Xie, G., Liu, M., Olson, J. S., Fabian, M., Dooley, D. M., and Lei, B. (2008) Pathway for heme uptake from human methemoglobin by the iron-regulated surface determinants system of Staphylococcus aureus. *J. Biol. Chem.* 283, 18450–18460.
- (10) Murvoy, N., Tiedemann, M. T., Pluym, M., Cheung, J., Heinrichs, D. E., and Stillman, M. J. (2008) Demonstration of the iron-regulated surface determinant (Isd) heme transfer pathway in Staphylococcus aureus. *J. Biol. Chem.* 283, 28125–28136.
- (11) Tiedemann, M. T., Heinrichs, D. E., and Stillman, M. J. (2012) Multiprotein heme shuttle pathway in Staphylococcus aureus: iron-regulated surface determinant cog-wheel kinetics. *J. Am. Chem. Soc.* 134, 16578–16585.
- (12) Murvoy, N., Tiedemann, M. T., Pluym, M., Cheung, J., Heinrichs, D. E., and Stillman, M. J. (2008) Crystal structure of the heme-IsdC complex, the central conduit of the Isd iron/heme uptake system in Staphylococcus aureus. *J. Biol. Chem.* 283, 28125–28136.
- (13) Aranda, IV, R., Worley, C. E., Liu, M., Bitto, E., Cates, M. S., Olson, J. S., Lei, B., and Phillips, G. N., Jr. (2007) Bis-methionyl coordination in the crystal structure of the heme-binding domain of the streptococcal cell surface protein Shp. *J. Mol. Biol.* 374, 374–383.
- (14) Pilpa, R. M., Fadeev, E. A., Villareal, V. A., Wong, M. L., Phillips, M., and Clubb, R. T. (2006) Solution structure of the NEAT (NEAR Transporter) domain from IsdH/HarA: the human hemoglobin receptor in Staphylococcus aureus. *J. Mol. Biol.* 360, 435–447.
- (15) Grigg, J. C., Vermeiren, C. L., Heinrichs, D. E., and Murphy, M. E. (2007) Haem recognition by a Staphylococcus aureus NEAT domain. *Mol. Microbiol.* 63, 139–149.
- (16) Sharp, K. H., Schneider, S., Cockayne, A., and Paoli, M. (2007) Crystal structure of the heme-IsdC complex, the central conduit of the Isd iron/heme uptake system in Staphylococcus aureus. *J. Biol. Chem.* 282, 10625–10631.
- (17) Pilpa, R. M., Robson, S. A., Villareal, V. A., Wong, M. L., Phillips, M., and Clubb, R. T. (2009) Functionally distinct NEAT (NEAR Transporter) domains within the Staphylococcus aureus IsdH/HarA protein extract heme from methemoglobin. *J. Biol. Chem.* 284, 1166–1176.
- (18) Villareal, V. A., Pilpa, R. M., Robson, S. A., Fadeev, E. A., and Clubb, R. T. (2008) The IsdC protein from Staphylococcus aureus uses a flexible binding pocket to capture heme. *J. Biol. Chem.* 283, 31591–31600.
- (19) Nygaard, T. K., Blouin, G. C., Liu, M., Fukumura, M., Olson, J. S., Fabian, M., Dooley, D. M., and Lei, B. (2006) The mechanism of direct heme transfer from the streptococcal cell surface protein Shp to HtsA of the HtsABC transporter. *J. Biol. Chem.* 281, 20761–20771.
- (20) Ran, Y., Zhu, H., Liu, M., Fabian, M., Olson, J. S., Aranda, R., Phillips, G. N., Jr., Dooley, D. M., and Lei, B. (2007) Bis-methionine ligation to heme iron in the streptococcal cell surface protein Shp facilitates rapid hemin transfer to HtsA of the HtsABC transporter. *J. Biol. Chem.* 282, 31380–31388.
- (21) Liu, M., Tanaka, W. N., Zhu, H., Xie, G., Dooley, D. M., and Lei, B. (2008) Direct hemin transfer from IsdA to IsdC in the iron-regulated surface determinant (Isd) heme acquisition system of Staphylococcus aureus. *J. Biol. Chem.* 283, 6668–6676.
- (22) Lei, B. (2010) Benfang Lei's research on heme acquisition in Gram-positive pathogens and bacterial pathogenesis. *World J. Biol. Chem.* 1, 286–290.
- (23) Lei, B., Smoot, L. M., Menning, H. M., Voyich, J. M., Kala, S. V., Deleo, F. R., Reid, S. D., and Musser, J. M. (2002) Identification and characterization of a novel heme-associated cell surface protein made by Streptococcus pyogenes. *Infect. Immun.* 70, 4494–4500.
- (24) Lei, B., Liu, M., Voyich, J. M., Prater, C. L., Kala, S. V., DeLeo, F. R., and Musser, J. M. (2003) Identification and characterization of HtsA, a second heme-binding protein made by Streptococcus pyogenes. *Infect. Immun.* 71, 5962–5969.
- (25) Bates, C. S., Montanez, G. E., Woods, C. R., Vincent, R. M., and Eichenbaum, Z. (2003) Identification and characterization of a Streptococcus pyogenes operon involved in binding of hemoproteins and acquisition of iron. *Infect. Immun.* 71, 1042–1055.
- (26) Zhu, H., Liu, M., and Lei, B. (2008) The surface protein Shr of Streptococcus pyogenes binds heme and transfers it to the streptococcal heme-binding protein Shp. *BMC Microbiol.* 8, 15.
- (27) Fabian, M., Solomaha, E., Olson, J. S., and Maresso, A. W. (2009) Heme transfer to the bacterial cell envelope occurs via a secreted hemophore in the Gram-positive pathogen Bacillus anthracis. *J. Biol. Chem.* 284, 32138–32146.
- (28) Ran, Y., Liu, M., Zhu, H., Nygaard, T. K., Brown, D. E., Fabian, M., Dooley, D. M., and Lei, B. (2010) Spectroscopic identification of heme axial ligands in HtsA that are involved in heme acquisition by Streptococcus pyogenes. *Biochemistry* 49, 2834–2842.
- (29) Fuhrhop, J. H., and Smith, K. M. (1975) in *Porphyrins and Metalloporphyrins* (Smith, K. M., Ed.) pp 804–807, Elsevier Publishing, New York.
- (30) Eswar, N., Eramian, D., Webb, B., Shen, M. Y., and Sali, A. (2008) Protein structure modeling with MODELLER. *Methods Mol. Biol.* 426, 145–159.
- (31) Eswar, N., Webb, B., Marti-Renom, M. A., Madhusudhan, M. S., Eramian, D., Shen, M. Y., Pieper, U., and Sali, A. (2007) Comparative Protein Structure Modeling Using MODELLER. *Curr. Protoc. Bioinformatics* 50, 2.9.1–2.9.31.
- (32) Lyskov, S., and Gray, J. J. (2008) The RosettaDock server for local protein-protein docking. *Nucleic Acids Res. Suppl.* 36 (2), W233–W238.
- (33) Grigg, J. C., Vermeiren, C. L., Heinrichs, D. E., and Murphy, M. E. (2007) Heme coordination by Staphylococcus aureus IsdE. *J. Biol. Chem.* 282, 28815–28822.
- (34) Barker, P. D., Nerou, E. P., Cheesman, M. R., Thomson, A. J., de Oliveira, P., and Hill, H. A. (1996) Bis-methionine ligation to heme iron in mutants of cytochrome b562. 1. Spectroscopic and electrochemical characterization of the electronic properties. *Biochemistry* 35, 13618–13626.
- (35) Villareal, V. A., Spirig, T., Robson, S. A., Liu, M., Lei, B., and Clubb, R. T. (2011) Transient weak protein-protein complexes transfer heme across the cell wall of Staphylococcus aureus. *J. Am. Chem. Soc.* 133, 14176–14179.
- (36) Abe, R., Caaveiro, J. M., Kozuka-Hata, H., Oyama, M., and Tsumoto, K. (2012) Mapping ultra-weak protein-protein interactions between heme transporters of Staphylococcus aureus. *J. Biol. Chem.* 287, 16477–16487.
- (37) Krieg, S., Huche, F., Diederichs, K., Izadi-Pruneyre, N., Lecroisey, A., Wandersman, C., Delepelaire, P., and Welte, W. (2009) Heme uptake across the outer membrane as revealed by crystal structures of the receptor–hemophore complex. *Proc. Natl. Acad. Sci. U. S. A.* 106, 1045–1050.
- (38) Spirig, T., Malmirchegini, G. R., Zhang, J., Robson, S. A., Sjødt, M., Liu, M., Krishna Kumar, K., Dickson, C. F., Gell, D. A., Lei, B., Loo, J. A., and Clubb, R. T. (2013) Staphylococcus aureus uses a novel multidomain receptor to break apart human hemoglobin and steal its heme. *J. Biol. Chem.* 288, 1065–1078.
- (39) Cobessi, D., Meksem, A., and Brillet, K. (2010) Structure of the heme/hemoglobin outer membrane receptor ShuA from Shigella

dysenteriae: heme binding by an induced fit mechanism. *Proteins* 78, 286–294.

(40) Olczak, T. (2006) Analysis of conserved glutamate residues in *Porphyromonas gingivalis* outer membrane receptor HmuR: toward a further understanding of heme uptake. *Arch. Microbiol.* 186, 393–402.

(41) Liu, X., Olczak, T., Guo, H. C., Dixon, D. W., and Genco, C. A. (2006) Identification of amino acid residues involved in heme binding and hemoprotein utilization in the *Porphyromonas gingivalis* heme receptor HmuR. *Infect. Immun.* 74, 1222–1232.

(42) Caillet-Saguy, C., Piccioli, M., Turano, P., Izadi-Pruneyre, N., Delepierre, M., Bertini, I., and Lecroisey, A. (2009) Mapping the interaction between the hemophore HasA and its outer membrane receptor HasR using CRINEPT-TROSY NMR spectroscopy. *J. Am. Chem. Soc.* 131, 1736–1744.

(43) Honsa, E. S., Owens, C. P., Goulding, C. W., and Maresso, A. W. (2013) The near-iron transporter (NEAT) domains of the anthrax hemophore IsdX2 require a critical glutamine to extract heme from methemoglobin. *J. Biol. Chem.* 288, 8479–90.